

Article

Ultrasound-Guided Photoacoustic Imaging of Salivary Gland Hemodynamics in Rabbits

Eftekhar Rajab Bolookat^{1,2}, Vui King Vincent-Chong¹ , Laurie J. Rich^{1,3}, Anurag K. Singh⁴ and Mukund Seshadri^{1,5,*} 

- ¹ Department of Oral Oncology, Roswell Park Comprehensive Cancer Center, Buffalo, NY 14263, USA; eftekhar.rajabbolookat@unhealth.unc.edu (E.R.B.); vincentvuiqing.chong@roswellpark.org (V.K.V.-C.); laurie.rich@fujifilm.com (L.J.R.)
- ² Department of Radiation Oncology, University of North Carolina—School of Medicine, Chapel Hill, NC 27599, USA
- ³ Fujifilm Visualsonics Corporation, Toronto, ON M4N 3N1, Canada
- ⁴ Department of Radiation Medicine, Roswell Park Comprehensive Cancer Center, Buffalo, NY 14263, USA; anurag.singh@roswellpark.org
- ⁵ Department of Radiology—Medical Physics Program, University at Buffalo-Jacobs School of Medicine and Biomedical Sciences, Buffalo, NY 14203, USA
- * Correspondence: mukund.seshadri@roswellpark.org; Tel.: +1-716-845-1552

Abstract: Xerostomia (severe dry mouth) is a debilitating and often permanent side effect experienced by head and neck cancer patients due to radiation injury to salivary glands. In this study, we evaluated the potential of ultrasound (US)-guided photoacoustic imaging (PAI) to non-invasively assess early changes in salivary gland hemodynamics following radiation therapy (RT). US-guided PAI was performed in New Zealand white rabbits to visualize and quantify the hemoglobin concentration (HbT) and oxygen saturation (%sO₂) of parotid glands before and after RT. The imaging findings were validated with histology and sialometry. An early increase in parotid gland HbT and %sO₂ was seen following RT. Consistent with the PAI observations, histology of salivary glands revealed dilated blood vessels, along with hemorrhaging and fibrosis. Sialometric analysis confirmed a significant reduction in stimulated saliva secretion in irradiated rabbits compared to controls. Collectively, our findings demonstrate the translational utility of US-guided PAI as a valuable tool for label-free functional imaging of salivary gland hemodynamics in vivo.

Keywords: photoacoustic imaging; salivary glands; ultrasound; radiation therapy; xerostomia



Citation: Bolookat, E.R.; Vincent-Chong, V.K.; Rich, L.J.; Singh, A.K.; Seshadri, M. Ultrasound-Guided Photoacoustic Imaging of Salivary Gland Hemodynamics in Rabbits. *Photonics* **2024**, *11*, 273. <https://doi.org/10.3390/photonics11030273>

Received: 19 January 2024
Revised: 2 March 2024
Accepted: 11 March 2024
Published: 20 March 2024



Copyright: © 2024 by the authors. Licensee MDPI, Basel, Switzerland. This article is an open access article distributed under the terms and conditions of the Creative Commons Attribution (CC BY) license (<https://creativecommons.org/licenses/by/4.0/>).

1. Introduction

The importance of salivary secretion in the maintenance of oral and systemic health is well recognized [1]. In head and neck cancer patients, salivary gland dysfunction is a common and often permanent side effect due to radiation injury to the glands and is associated with a subjective sensation of dry mouth (xerostomia) and an objective reduction in saliva secretion [2]. As a consequence, patients experience a marked reduction in their quality of life due to compromised speech, eating and swallowing function. Additionally, radiation-induced xerostomia (RIX) increases patients' susceptibility to oral infection and dental caries [2,3].

A consistent body of research in experimental models has implicated vascular injury to the salivary glands as a major contributor to RIX [3–5]. These experimental studies have typically utilized immunohistochemical markers of vascularity (e.g., CD31) to assess the vascular changes in salivary glands following radiation therapy [6,7]. Furthermore, a majority of these investigations have been conducted using the laboratory mouse (*mus musculus*) to understand the radiobiology of salivary glands [3–6]. Although mouse models are useful, differences in anatomy, histology and physiology between murine and

human salivary glands can limit the extrapolation of findings [7,8]. The development and application of non-invasive functional imaging methods to monitor salivary gland injury in a clinically relevant large animal model could overcome these limitations, provide mechanistic insight, and potentially enable early detection of salivary gland dysfunction.

In this regard, the New Zealand white (NZW) rabbit has been previously utilized as a translational model to examine salivary gland biology and function [9,10]. Scintigraphic studies have been conducted in NZW rabbits to assess radiation-induced salivary gland injury and to evaluate the efficacy of radioprotective agents such as lidocaine [11,12]. Although conventional scintigraphy provides quantitative estimates of gland function, it is invasive and requires the use of radioisotopes. To overcome these limitations, we have been examining the potential of ultrasound (US)-guided photoacoustic imaging (PAI) for combined structural and functional imaging of radiation-induced salivary gland injury. While US relies on differences in acoustic impedance between tissues [13], PAI exploits the optical absorption characteristics of endogenous chromophores such as hemoglobin (Hb) to provide quantitative measures of the hemoglobin concentration (HbT) and oxygen saturation (%sO₂) [14,15]. Our studies in murine models have validated US-PAI measures of salivary gland hemodynamics with histology and demonstrated the strong correlation between a vascular response to parasympathetic stimulation or blockade and saliva secretion [16,17]. Recently, we have also examined the ability of US-PAI to monitor the early and late vascular response of murine salivary glands to radiation [18]. However, to the best of our knowledge, the safety and performance of US-PAI for evaluation of salivary gland hemodynamics in rabbits has not been evaluated. To address this gap in knowledge, we conducted experimental imaging studies in NZW rabbits to assess changes in parotid gland hemodynamics following radiation. The parotid gland was chosen, as it is most commonly affected by radiation in head and neck cancer patients. Imaging findings were validated with histology and sialometry.

2. Materials and Methods

2.1. Rabbits

Adult male, specific-pathogen free, New Zealand White (NZW) rabbits ranging from 1.5 to 2 kg were purchased from Charles River Corporation (Saint Constant, QC, Canada). Rabbits were fed high-fiber diet (Rabbit diet # 2031; Harlan Teklad, KY, USA) and purified water and were housed in individual stainless-steel cages containing noncontact bedding under 12 h light and dark cycles. Environmental enrichment in the form of manipulanda was provided (Bio-Serv, Flemington, NY, USA).

2.2. Radiation Procedure

Rabbits were anesthetized using 2% isoflurane via inhalation through a mask. Radiation was delivered to the parotid glands (using two opposing lateral fields) using an orthovoltage X-ray unit (Philips RT 250 Philips Medical Systems, Andover, MA, USA) equipped with an aluminum filter running at 250 kV/17.7 mA. The dose rate of the unit at these settings was ~0.68 Gy/min. Animals were monitored with a closed-circuit TV during irradiation and observed after completion of treatment to ensure full recovery.

2.3. Ultrasound with Co-Registered Photoacoustic Imaging

Ultrasound (US) with co-registered photoacoustic imaging (PAI) of the rabbit parotid glands was performed using a commercially available 21 MHz linear array transducer system (Vevo LAZR; Fujifilm Visual Sonics Inc., Toronto, ON, Canada). The system consists of a tunable NIR Nd: YAG laser connected to a 256-element fiber-optic linear array hybrid US transducer. Three-dimensional B-mode US images were acquired to calculate gland volume and used to guide PAI acquisition. PA datasets were acquired for a single central slice of the gland using the following parameters: transducer: LZ-250, frequency: 21 MHz, wavelength: 750/850 nm, acquisition mode: OxyHemo; HbT threshold 20%. Animals were monitored closely during the imaging procedure and following completion of imaging

until recovery. Imaging datasets were processed offline using the Vevo LAB software using a dedicated workstation. Parametric maps of HbT and %sO₂ were reconstructed using the built-in algorithm based on the two-wavelength approach [16]. US-based estimates of gland volume and PAI-based relative estimates of HbT, %sO₂ tot (representing average oxygen saturation values for all pixels within the salivary gland region of interest (ROI), are reported.

2.4. Sialometry

Saliva production was quantified following stimulation with the parasympathetic agonist pilocarpine (1 mg/kg) over a 7 min period. Saliva was collected every 2 min for 7 min by placing a pre-weighed strip of filter paper into the oral cavity for 90 s and then removing the paper to be re-weighed.

2.5. Histopathology

Salivary glands were collected from control and irradiated rabbits and placed in zinc fixative. Glass slides containing hematoxylin and eosin (H&E)-stained sections were scanned and digitized using the ScanScopeXT system (Aperio Technologies, Vista, CA, USA).

2.6. Statistics

All statistical analysis and graphical display of data were performed using GraphPad Prism (GraphPad Software, Version 9.00 for Windows, San Diego, CA, USA). Two-way repeated measures ANOVA with multiple comparisons was performed to compare differences between control and irradiated glands (gland volume, PAI and sialometry). Correlation between US/PAI measurements and saliva secretion was examined using Pearson analysis. *p*-values of <0.05 were considered statistically significant.

3. Results

The design of our experimental study is shown in Figure 1. Naïve male NZW rabbits (control *n* = 3; RT *n* = 4) underwent US-guided PAI of the parotid glands at baseline and 1 week post radiation therapy (RT; 15 Gy). Changes in salivary gland volume (US) along with HbT/%sO₂ (PAI) were obtained and validated using quantitative measures of saliva secretion following pilocarpine stimulation and ex-vivo histologic assessment of the glands. The experimental design for US-guided PAI is shown in Figure 1.

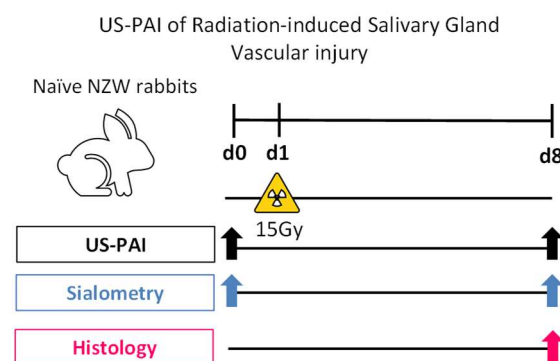


Figure 1. Study design for US-PAI-based assessment of salivary gland hemodynamics in rabbits. Naïve male NZW rabbits underwent US-guided PAI of the parotid glands at baseline prior to radiation. Animals in the radiation arm received a single dose of 15 Gy to the parotid glands and follow-up imaging examination was performed 1 week post radiation. Imaging data was validated using sialometry and histology.

Anesthetized rabbits were placed on a heated platform for imaging, as shown in Figure 2 (left). The digital photographs presented in Figure 2 also illustrate the trans-

ducer position (left) and the imaging plane (middle). Given the superficial location of the glands, B-mode US allowed for adequate visualization of the parotid gland in rabbits (Figure 2, right).

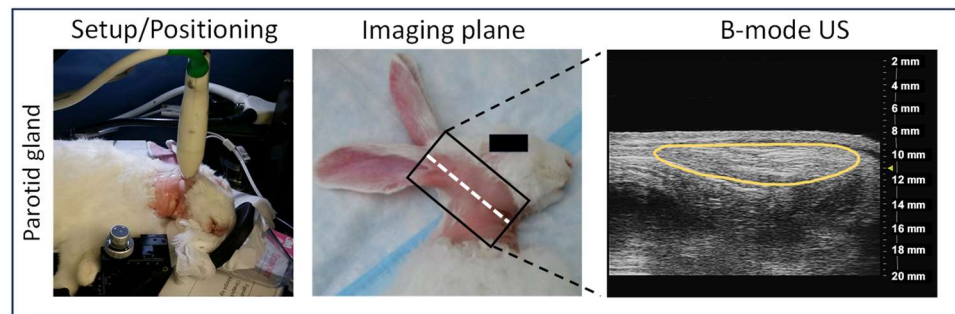


Figure 2. Experimental setup for US-PAI of parotid glands in rabbits. (Left) Digital photograph showing positioning of the anesthetized rabbit on a heated platform for imaging of the parotid glands. (Middle) Digital photograph illustrating transducer positioning and imaging plane. (Right) B-mode US image of the parotid gland in a NZW rabbit. The gland is outlined in yellow. The superficial location of the parotid gland enabled successful visualization of the glands with US-guided PAI.

We performed US-guided PAI to assess the hemodynamics of the parotid glands in rabbits at baseline and post RT. The panel of images shown in Figure 3 represent pseudocolored parametric maps of HbT and %sO₂ of parotid glands overlaid on the B-mode US images for rabbits in the control and irradiated rabbits at baseline (d0) and at 1 week post radiation (d8). Blue pixels represent areas of low HbT/%sO₂ signal, while red pixels represent areas of high HbT/%sO₂ signal within the gland. The parotid gland is outlined in white on the images.

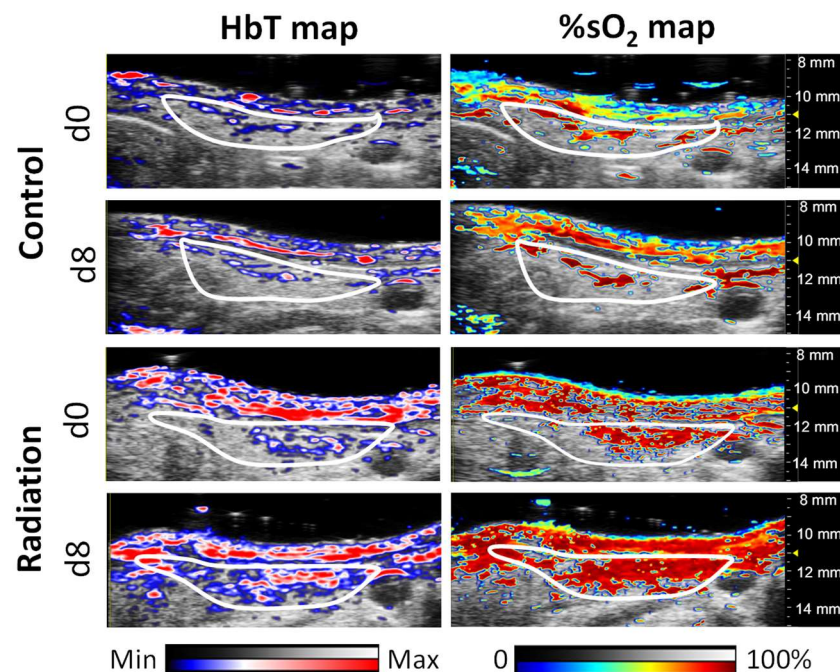


Figure 3. PAI-based mapping of salivary gland hemodynamics in rabbits. The panel of images represents reconstructed HbT and sO₂ maps of the parotid glands in control and irradiated rabbits at baseline (d0) and at 1 week post radiation (d8). Pseudocolored PA images overlaid on the B-mode US images are shown. The parotid gland is outlined in white on the images.

As is evident from the HbT and sO₂ maps, adequate PA signal was detected from the salivary glands of all rabbits at baseline. Qualitative visual examination of the HbT

and oxy-sat maps did not reveal any difference in the gland hemodynamics of control rabbits between d0 and d8. In comparison, a marked increase in the HbT and oxy-sat signal was seen in the parotid gland of irradiated rabbits on d8, suggestive of radiation-induced disruption of the gland vasculature.

The parotid gland volumes (US) and HbT/%sO₂ (PAI) were calculated from the images. As shown in Figure 4, three-dimensional B-mode US revealed a significant reduction in the parotid gland volume in irradiated rabbits compared to controls on Day 8 ($p < 0.001$), which is consistent with clinical observations reported in head and neck cancer patients. The relative estimates of HbT (Figure 4B) confirmed our visual assessment and revealed a significant increase ($p < 0.05$) in the parotid gland HbT of irradiated animals compared to controls on Day 8. The relative estimates of %sO₂ were calculated from the PA images. Specifically, %sO₂ tot reports the oxygen saturation values of all pixels within the parotid gland ROI and is reflective of the oxygenation status of the whole gland. Consistent with the increased HbT, we observed a significant increase in %sO₂ tot values on Day 8, suggestive of vasodilation or pooling of blood within the glands following RT (Figure 4C).

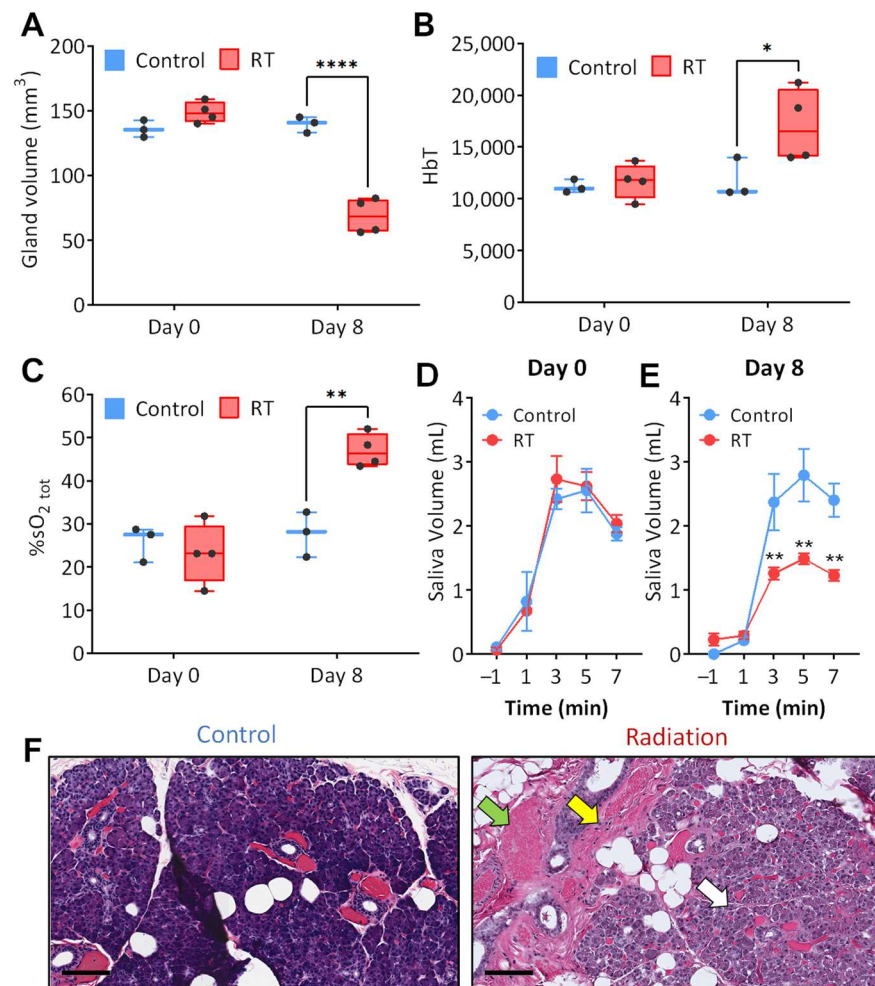


Figure 4. Quantitative US-PAI analysis of radiation-induced salivary injury in rabbits. Box and whisker plots show US-based estimates of parotid gland volume (A), along with PAI-based relative estimates of gland HbT (B) and %sO₂ (C) for rabbits in control and RT groups. (D,E) Temporal curves of saliva secretion before and after stimulation with pilocarpine on Day 0 (D) and Day 8 (E) in control and irradiated rabbits. (F) Hematoxylin and eosin-stained sections (H&E) of parotid glands from control and irradiated rabbits (20× magnification; scale bar 100 μm) on Day 8. * $p < 0.05$; ** $p < 0.01$; **** $p < 0.0001$.

To assess the impact of radiation-induced vascular damage on gland function, we measured the stimulated salivary secretion levels in the control and irradiated rabbits using the parasympathetic agonist, pilocarpine. At baseline (Day 0), the temporal curves of saliva volume revealed comparable saliva production by rabbits in both arms in response to pilocarpine stimulation (Figure 4D). In comparison, a significant reduction in saliva volume was observed in the irradiated animals on Day 8 compared to controls (Figure 4E). Ex vivo histologic assessment was also performed on excised glands on Day 8 to validate the US-PAI observations. As shown in Figure 4F, hematoxylin and eosin (H&E)-stained sections of irradiated rabbits provided evidence of acinar atrophy (white arrow) and a reduction in zymogen granules in irradiated parotid glands. Consistent with our HbT and sO₂ maps and quantitative measurements, the H&E sections revealed the presence of vasodilation, congestion, hemorrhaging (green arrow), and fibrosis (yellow arrow) in response to RT.

Finally, we examined the correlation between gland volume, HbT, %sO₂ and saliva secretion (Figure 5). Pooled analysis of the data from control and irradiated rabbits at both time points revealed a negative correlation between gland volume–HbT (Figure 5A) and gland volume–%sO₂ (Figure 5B). This relationship between gland volume–HbT (Pearson $r = -0.82$; $p = 0.003$) and gland volume–%sO₂ (Pearson $r = -0.89$; $p = 0.002$) was maintained when considering irradiated rabbits alone at both timepoints. No correlation was seen between the gland volume and PAI indices in the control rabbits ($p > 0.05$). A positive correlation was seen between HbT and %sO₂ values (Pearson $r = 0.85$; $p < 0.0001$) in all rabbits (Figure 5C).

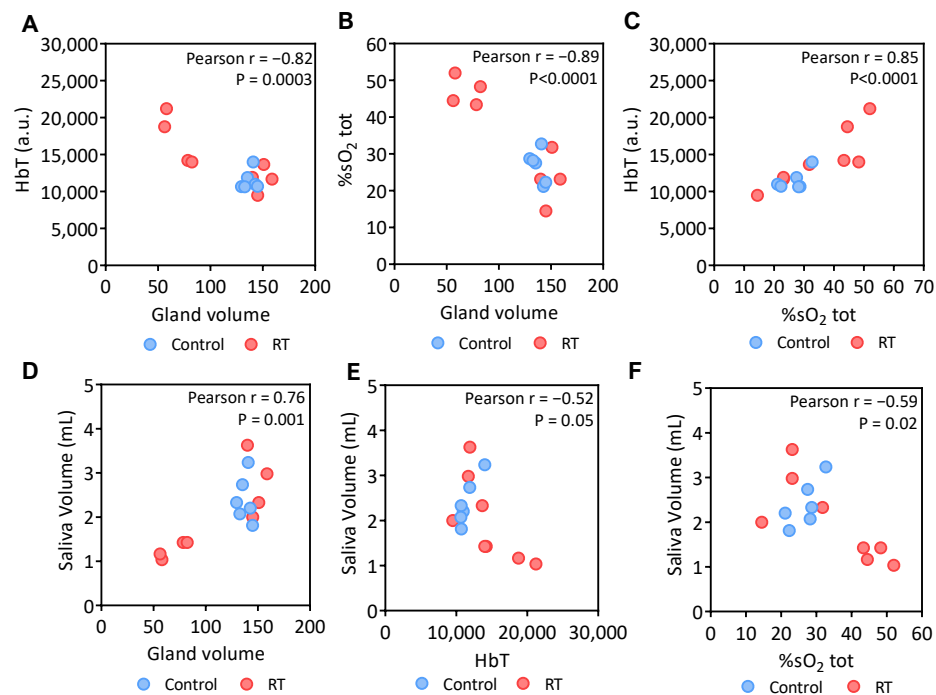


Figure 5. Relationship between parotid gland volume, hemodynamics and saliva secretion. Correlation plots illustrate association between parotid gland volume–HbT (A), gland volume–%sO₂ (B), HbT–%sO₂ (C), saliva secretion–gland volume (D), saliva secretion–gland HbT (E), and saliva secretion–%sO₂ (F) for all rabbits (control and irradiated) at both time points (d0 and d8). Saliva secretion measured at 3 min post pilocarpine stimulation was utilized. Control rabbits are shaded in blue, and irradiated rabbits are shaded in red. Pearson r values and p values are shown within each plot.

A comparative evaluation of the PAI data to sialometry in the control rabbits did not reveal any association between gland volume and stimulated saliva secretion ($p > 0.05$). In comparison, a positive correlation was seen between parotid gland HbT and saliva

secretion in the control rabbits (Pearson $r = 0.92$; $p = 0.007$). A pooled analysis showed a positive correlation (Pearson $r = 0.76$; $p = 0.001$) between saliva secretion–gland volume (Figure 5D) and a negative correlation between saliva secretion–HbT (Pearson $r = -0.52$; $p = 0.05$, Figure 5E) and saliva secretion–%sO₂ (Pearson $r = -0.59$; $p = 0.02$, Figure 5F). The negative correlation between saliva secretion–%sO₂ was stronger when considering irradiated rabbits alone (Pearson $r = -0.76$; $p = 0.02$).

4. Discussion

We have recently demonstrated the potential of PAI to non-invasively monitor radiation injury in murine models [18]. Building on our previous work, in the present study, we assessed acute changes in parotid gland hemodynamics (HbT/sO₂) following radiation treatment in rabbits. Our rationale for investigating the utility of PAI in rabbits is multi-fold. First, the anatomy of the rabbit salivary glands is similar to humans, unlike that of mice, in which the glands form a complex. Second, the rabbit model allows us to replicate the radiation therapy workflow that is typically used in the clinical setting. And finally, given that the imaging depth in PAI is limited by light attenuation, an evaluation of the performance of PAI in a clinically relevant large animal model would allow us to better assess its potential clinical utility.

Our study focused on understanding the radiation response of parotid glands, a major contributor to saliva secretion in humans. We performed PAI of the rabbit parotid glands under US guidance. Our previous studies in tissue-mimicking phantoms [19] and in vivo [20] studies have demonstrated that PAI can reliably detect hemodynamic parameters up to ~3 cm in tissue. Given the superficial location of the salivary glands (Figure 2), light penetration was not an issue, and an adequate PAI signal was detected in the parotid glands in all rabbits. No change in parotid gland hemodynamics (HbT/%sO₂) was observed in control rabbits between the two imaging sessions (d0 and d8), highlighting the reliability of PAI. These results, along with our published studies in mice [16–18], confirm the ability of PAI to reliably measure salivary gland hemodynamics.

To date, a comparative assessment of the salivary gland radiation response between mice and rabbits has not been reported. In our previous study [18], immunocompetent mice exposed to a single high dose of radiation did not show any change in HbT or %sO₂ at 1 week post RT. In comparison, we observed an increase in HbT and %sO₂ at 1 week post RT in rabbits, which suggests that the kinetics of radiation-induced vascular injury may vary between rabbits and mice. However, it is important to recognize that several confounding variables, including differences in the physiology of mice and rabbits, pose a challenge in direct comparison of the two studies. In addition to the anatomic differences, the radiation dose tolerance and dose sensitivity of the salivary glands may likely vary between the two species.

Histologic analysis revealed hemorrhaging in the rabbit parotid glands post RT, validating our PAI findings. Sialometric assessment also confirmed a reduction in saliva secretion following radiation. We observed a positive correlation between saliva secretion and gland volume and a negative correlation between saliva secretion–HbT/%sO₂. Although further investigation into the mechanisms of radiation-induced vascular injury are warranted, our observations are consistent with a previous clinical study [21]. Using Doppler US, Wu et al. demonstrated lower vascular velocity, resistive and pulsatility indices in post-RT parotid glands compared to healthy salivary glands [21].

We recognize the limitations of our study. These include a relatively small sample size, a cross-sectional assessment of the vascular response to RT and that only a single dose of RT was studied in naïve rabbits. Nevertheless, our results provide important proof-of-concept to highlight the translational utility of US-guided PAI as a valuable tool for visualization of the salivary gland anatomy and functional imaging of the vascularity and oxygenation without the need for radioisotopes or intravenous contrast agents. We are currently examining the potential of integrating PAI into a clinically relevant workflow of image-guided RT, developed by us [22]. We are also focused on validating PAI-based

measures of tumor and salivary gland vascular response to RT with magnetic resonance imaging (MRI) in rabbits. We hope to report on our findings from these studies in the near future.

Author Contributions: E.R.B., A.K.S. and M.S. conceived and designed the research. E.R.B., L.J.R. and V.K.V.-C. performed all experiments and data analysis. All authors participated in the interpretation of data, writing and revision of the manuscript. M.S. provided administrative, technical or material support and supervised all aspects of the work. All authors have read and agreed to the published version of the manuscript.

Funding: This research was supported by grants from the National Cancer Institute (1R01CA204636), National Center for Research Resources (S10OD010393-01), Mark Diamond Research Fund and the Roswell Park Alliance Foundation. The research utilized shared resources supported by Roswell Park's Cancer Center Support Grant from the National Cancer Institute P30CA016056.

Institutional Review Board Statement: All experimental procedures were performed in accordance with an animal study protocol (1285 Rb) approved by The Institutional Animal Care and Use Committee (IACUC) at Roswell Park Comprehensive Cancer Center.

Informed Consent Statement: Not applicable.

Data Availability Statement: All data needed to evaluate the conclusions are presented in the paper. Raw data that support the findings of the study are available from the corresponding author upon reasonable request.

Acknowledgments: The authors acknowledge the technical assistance provided by the following shared resources at Roswell Park Comprehensive Cancer Center: Laboratory Animal Shared Resource, Translational Imaging Shared Resource and the Pathology Resource Network.

Conflicts of Interest: L.J.R. is currently an employee of Fujifilm-VisualSonics Corporation. The remaining authors declare no competing financial interests. The funding sponsors had no role in the design of the study, collection, analyses, or interpretation of data, writing of the manuscript, and in the decision to publish the results.

References

1. Edgar, W.M. Saliva: Its secretion, composition and functions. *Br. Dent. J.* **1992**, *172*, 305–312. [[CrossRef](#)]
2. Vistoso Monreal, A.; Polonsky, G.; Shiboski, C.; Sankar, V.; Villa, A. Salivary Gland Dysfunction Secondary to Cancer Treatment. *Front. Oral Health* **2022**, *3*, 907778. [[CrossRef](#)] [[PubMed](#)]
3. Chambers, M.S.; Garden, A.S.; Kies, M.S.; Martin, J.W. Radiation-induced xerostomia in patients with head and neck cancer: Pathogenesis, impact on quality of life, and management. *Head Neck* **2004**, *26*, 796–807. [[CrossRef](#)] [[PubMed](#)]
4. Mizrachi, A.; Cotrim, A.P.; Katabi, N.; Mitchell, J.B.; Verheij, M.; Haimovitz-Friedman, A. Radiation-Induced Microvascular Injury as a Mechanism of Salivary Gland Hypofunction and Potential Target for Radioprotectors. *Radiat. Res.* **2016**, *186*, 189–195. [[CrossRef](#)] [[PubMed](#)]
5. Jasmer, K.J.; Gilman, K.E.; Muñoz Forti, K.; Weisman, G.A.; Limesand, K.H. Radiation-Induced Salivary Gland Dysfunction: Mechanisms, Therapeutics and Future Directions. *J. Clin. Med.* **2020**, *9*, 4095. [[CrossRef](#)] [[PubMed](#)]
6. Kim, J.Y.; An, C.H.; Kim, J.Y.; Jung, J.K. Experimental Animal Model Systems for Understanding Salivary Secretory Disorders. *Int. J. Mol. Sci.* **2020**, *21*, 8423. [[CrossRef](#)]
7. Maruyama, C.L.; Monroe, M.M.; Hunt, J.P.; Buchmann, L.; Baker, O.J. Comparing human and mouse salivary glands: A practice guide for salivary researchers. *Oral Dis.* **2019**, *25*, 403–415. [[CrossRef](#)]
8. Amano, O.; Mizobe, K.; Bando, Y.; Sakiyama, K. Anatomy and histology of rodent and human major salivary glands: -overview of the Japan salivary gland society-sponsored workshop-. *Acta Histochem. Cytochem.* **2012**, *45*, 241–250. [[CrossRef](#)]
9. Stammers, K.; Skagers, A.; Pastars, K.; Tomisheva, N.; Ratniece, M. Functional activity of rabbit salivary glands in reduced and restored regional arterial blood supply conditions. *Stomatologija* **2010**, *12*, 28–32.
10. Hakim, S.G.; Jacobsen, H.C.; Hermes, D.; Kosmehl, H.; Lauer, I.; Nadrowitz, R.; Sieg, P. Early immunohistochemical and functional markers indicating radiation damage of the parotid gland. *Clin. Oral Investig.* **2004**, *8*, 30–35. [[CrossRef](#)] [[PubMed](#)]
11. Bohuslavizki, K.H.; Brenner, W.; Klutmann, S.; Hübner, R.H.; Lassmann, S.; Feyerabend, B.; Lüttges, J.; Tinnemeyer, S.; Clausen, M.; Henze, E. Radioprotection of salivary glands by amifostine in high-dose radioiodine therapy. *J. Nucl. Med.* **1998**, *39*, 1237–1242.
12. Hakim, S.G.; Benedek, G.A.; Su, Y.X.; Jacobsen, H.C.; Klinger, M.; Dendorfer, A.; Hemmelmann, C.; Meller, B.; Nadrowitz, R.; Rades, D.; et al. Radioprotective effect of lidocaine on function and ultrastructure of salivary glands receiving fractionated radiation. *Int. J. Radiat. Oncol. Biol. Phys.* **2012**, *82*, e623–e630. [[CrossRef](#)]

13. Kaproth-Joslin, K.A.; Nicola, R.; Dogra, V.S. The History of US: From Bats and Boats to the Bedside and Beyond: RSNA Centennial Article. *Radiographics* **2015**, *35*, 960–970. [[CrossRef](#)]
14. Kruger, R.A. Photoacoustic ultrasound. *Med. Phys.* **1994**, *21*, 127–131. [[CrossRef](#)]
15. Li, C.; Wang, L.V. Photoacoustic tomography and sensing in biomedicine. *Phys. Med. Biol.* **2009**, *54*, R59–R97. [[CrossRef](#)]
16. Rich, L.J.; Seshadri, M. Photoacoustic imaging of salivary glands. *Biomed. Opt. Express* **2015**, *6*, 3157–3162. [[CrossRef](#)]
17. Rich, L.J.; Bolookat, E.R.; Seshadri, M. Dynamic photoacoustic imaging of neurovascular coupling in salivary glands. *J. Oral Biosci.* **2019**, *61*, 236–241. [[CrossRef](#)] [[PubMed](#)]
18. Bolookat, E.R.; Rich, L.J.; Vincent-Chong, V.K.; DeJohn, C.R.; Merzianu, M.; Hershberger, P.A.; Singh, A.K.; Seshadri, M. Noninvasive Monitoring of Radiation-Induced Salivary Gland Vascular Injury. *J. Dent. Res.* **2022**, *14*, 220345221138533. [[CrossRef](#)] [[PubMed](#)]
19. Rich, L.J.; Chamberlain, S.R.; Falcone, D.R.; Bruce, R.; Heinmiller, A.; Xia, J.; Seshadri, M. Performance Characteristics of Photoacoustic Imaging Probes with Varying Frequencies and Light-delivery Schemes. *Ultrason. Imaging* **2019**, *41*, 319–335. [[CrossRef](#)] [[PubMed](#)]
20. Rich, L.J.; Sexton, S.; Curtin, L.; Seshadri, M. Spatiotemporal Optoacoustic Mapping of Tumor Hemodynamics in a Clinically Relevant Orthotopic Rabbit Model of Head and Neck Cancer. *Transl. Oncol.* **2017**, *10*, 839–845. [[CrossRef](#)] [[PubMed](#)]
21. Wu, V.W.; Ying, M.T.; Kwong, D.L. Evaluation of radiation-induced changes to parotid glands following conventional radiotherapy in patients with nasopharyngeal carcinoma. *Br. J. Radiol.* **2011**, *84*, 843–849. [[CrossRef](#)] [[PubMed](#)]
22. Rajab Bolookat, E.; Malhotra, H.; Rich, L.J.; Sexton, S.; Curtin, L.; Sperryak, J.A.; Singh, A.K.; Seshadri, M. Development and Validation of a Clinically Relevant Workflow for MR-Guided Volumetric Arc Therapy in a Rabbit Model of Head and Neck Cancer. *Cancers* **2020**, *12*, 572. [[CrossRef](#)] [[PubMed](#)]

Disclaimer/Publisher’s Note: The statements, opinions and data contained in all publications are solely those of the individual author(s) and contributor(s) and not of MDPI and/or the editor(s). MDPI and/or the editor(s) disclaim responsibility for any injury to people or property resulting from any ideas, methods, instructions or products referred to in the content.